



Article

Assessing Interactions between Nitrogen Supply and Leaf Blast in Rice by Hyperspectral Imaging

Angeline Wanjiku Maina ¹, Mathias Becker ² and Erich-Christian Oerke ^{1,*}

¹ Institute for Crop Science and Resource Conservation (INRES)—Plant Pathology, Rheinische Friedrich-Wilhelms University of Bonn, 53121 Bonn, Germany; wanjiku.maina@uni-bonn.de

² Institute for Crop Science and Resource Conservation (INRES)—Plant Nutrition, Rheinische Friedrich-Wilhelms University of Bonn, 53121 Bonn, Germany; mathias.becker@uni-bonn.de

* Correspondence: ec-oerke@uni-bonn.de

Abstract: Mineral nitrogen (N) supply reportedly increases rice susceptibility to the fungal pathogen *Magnaporthe oryzae* causing blast disease. These biotic and abiotic factors cause changes in spectral reflectance of leaves; however, the effects of N × pathogen interactions on spectral characteristics of rice have not been studied. In this study, hyperspectral imaging was used to assess the effect of N supply on symptoms of rice leaf blast under greenhouse conditions. Three rice genotypes differing in blast susceptibility grown at low, medium, and high N supply were inoculated at the four-leaf stage with three *M. oryzae* isolates differing in virulence. The reflectance spectra (400 to 1000 nm) of healthy and symptomatic leaves were analyzed using the spectral angle mapper algorithm for supervised classification. Mineral N supply increased the contents of chlorophyll and total N. The number and area of lesions and total blast severity varied depending on rice genotype—*M. oryzae* isolate interactions and the amount of mineral N applied. The reflectance spectra of healthy tissue and of blast symptom subareas differed with N supply; rice genotypes differed in the response to N supply. Infected plants at high mineral N supply could be distinguished from those at low N supply due to higher differences in the spectra of symptom subareas. Results reveal the potential (and limitations) of hyperspectral imaging for quantifying N effects on rice leaves, disease severity, and symptom expression. The impact of these findings on plant phenotyping and remote sensing under field conditions is discussed.



Citation: Maina, A.W.; Becker, M.; Oerke, E.-C. Assessing Interactions between Nitrogen Supply and Leaf Blast in Rice by Hyperspectral Imaging. *Remote Sens.* **2024**, *16*, 939. <https://doi.org/10.3390/rs16060939>

Academic Editors: Marian-Daniel Iordache and Stephanie Delalieux

Received: 9 February 2024

Revised: 1 March 2024

Accepted: 4 March 2024

Published: 7 March 2024



Copyright: © 2024 by the authors. Licensee MDPI, Basel, Switzerland. This article is an open access article distributed under the terms and conditions of the Creative Commons Attribution (CC BY) license (<https://creativecommons.org/licenses/by/4.0/>).

Keywords: *Magnaporthe oryzae*; nitrogen application; *Oryza sativa*; spectral reflectance; symptom type

1. Introduction

Nitrogen (N) is essential for plant growth, and N deficiency is widely limiting rice production [1]. While N deficiency reduces crop productivity, excessive mineral N application can lead to negative environmental effects [2] and increases the impact of crop diseases caused by foliar pathogens [3]. Optimizing N application according to the crops' specific needs and through precision farming will not only enhance the N use efficiency but may also reduce the risk and the severity of crop diseases.

Mineral N fertilizer is known to affect the level of pathogen infection in plants, with higher N being correlated with increased host tissue susceptibility to diseases in wheat [4] and a number of other crops [5]. In rice, high N is reportedly associated with increased susceptibility to blast caused by the hemibiotrophic ascomycetous fungus *Magnaporthe oryzae* [6]. It is the most important pathogen in rice production worldwide, causing leaf and panicle blast, and resulting in yield losses [7]. Several studies have documented an increase in the severity of rice blast due to high N application rates [8,9]. High doses of N fertilizer accelerate plant growth, increasing the canopy density, thus creating a favorable microclimate for the development of the blast pathogen [6]. The effect of N on the disease is also mediated via an increased availability of nitrogenous compounds in rice tissues, which

are substrates for pathogen growth [5]. While high N supply stimulates the development of the pathogen [10], also a limited N availability to *M. oryzae* on plant surfaces reportedly stimulate the expression of effector genes, e.g., hydrophobin *MPG1*, thus increasing the blast susceptibility of rice [11].

The chemical methods currently used for assessing N in crops are destructive and involve tedious procedures [12]. The non-destructive determination of the leaf greenness (proxy for N content) by chlorophyll meter (SPAD-502) has increasingly replaced destructive sampling and chemical N analysis. However, such photometric measurements disregard leaf chlorosis caused by nutrients other than N (e.g., magnesium, sulfur, iron, zinc) and are limited to spectral bands at 650 and 940 nm, potentially overlooking important information in other regions of the spectrum [13]. SPAD may also fail to distinguish differences in N nutritional status of plants under high N conditions [12]. Likewise, conventional methods of monitoring plant diseases mainly rely upon visual plant inspection, which is time-consuming, labor-intensive, subjective, and unable to monitor the severity of diseases over large areas [14,15].

Optical sensing techniques provide a non-invasive and efficient way for evaluating both abiotic and biotic stresses in plants [14]. Non-imaging reflectance spectroscopy has proven effective in assessing both the crop's N status [16,17] and plant diseases [18,19]. However, this method averages spectral data over a field of view, without providing information on the spatial distribution of the measured parameters [20]. While low spatial resolutions may suffice to assess abiotic stresses that affect all plant parts, pathogen infections are highly restricted to specific plant tissues, at least in the early stages of epidemics, and consequently require high spatial resolutions of the sensing system.

Hyperspectral imaging (HSI) has proven to be an effective way to detect plant diseases as well as to monitor the nutritional status of crops [21,22]. It captures high-resolution spectral and spatial information of crops in the visible (VIS; 400 to 700 nm) and near-infrared (NIR; 700 to 1000 nm) ranges of the spectrum, which is associated with important biochemical and biophysical properties of the plant [23]. This technology detects rapidly and non-destructively changes in important indicators of plant health, such as the status of leaf pigments, the leaf water and nutrient contents, and leaf structure [15,24]. Numerous studies have documented HSI to effectively determine both the crop's nutritional status [25,26], and to diagnose plant diseases, including *Fusarium* in wheat [27], leaf diseases in sugar beet [28], and *Plasmopara viticola* in grapevine [21]. In rice, HSI has been used for assessing blast on panicles [29] and on leaves [30]. Maina and Oerke [31] demonstrated the suitability of HSI for assessing the gene-for-gene-specific interactions between genotypes of *Oryza sativa* and *M. oryzae*. These studies used HSI to assess either the crop nutrient status or plant diseases separately.

HSI provides spectral details for each pixel, enabling the assessment of spatial and spectral patterns of affected leaf tissues. While abiotic and biotic factors affect the same plant tissue at the same time, the mixed effect is displayed within the same pixel(s) of an image. Hyperspectral data have successfully discriminated combined stresses, e.g., symptoms caused by N deficiency and stripe rust infection in wheat [32], and the distribution of chlorophyll and carotenoids in cucumber leaves infected by angular leaf spot [33]. Liu and colleagues [34] successfully monitored wheat powdery mildew under different N levels using a spectrometer. Leaf rust-infected wheat leaves could be distinguished from N-deficient leaves because of the higher spatial variability of the chlorophyll fluorescence ratio at 686 and 740 nm [35]. Despite these promising reports for discriminating biotic and abiotic factors, no study to date has used HSI for simultaneously measuring the effects of different rates of N supply and of blast infection on rice, and generally on potential interactions of combinations of biotic and abiotic factors on spectral reflectance of rice tissues.

The hypothesis was that HSI can visualize and differentiate the effects of both mineral N supply, leaf blast infection, as well as their interactions. Consequently, HSI was applied to investigate the interactive effects of three mineral N application rates and of three *M. oryzae* isolates in three rice genotypes. Selected blast isolates differed in their virulence, while

rice genotypes differed in their blast resistance. The study addressed the following specific objectives: (i) determine growth responses, leaf chlorophyll and total N contents, and spectral leaf characteristics of rice genotypes at increasing mineral N supply; (ii) assess effects of mineral N supply on the severity of leaf blast; and (iii) quantify spectral variations of blast symptom subareas of rice genotypes subjected to different mineral N application rates. Ultimately, the study aimed at understanding the potential of HSI as an integrated tool for monitoring disease response in relation to the nutritional status of rice.

2. Materials and Methods

2.1. Origin and Cultivation of Rice and Blast Isolates

Three rice (*Oryza sativa* L.) genotypes were used in this study, comprising CO 39 (accession number IRGC 51231, obtained from IRRI, Philippines), IR64, and Nipponbare (provided by Michael Frei, Department for Plant Nutrition, University of Bonn). They represent the prevailing diversity of rice types and reported blast susceptibility, with CO 39 (*indica* type) representing the highly susceptible reference genotype, IR64 being a reportedly blast-resistant *indica* type, and Nipponbare being a susceptible *japonica* type.

Seeds were sown directly into pots (Ø 9 cm, height 6.8 cm) (Kausek, Mittenwalde, Germany), filled with 0.3 kg of loam soil at 5 seeds per pot. Plants were grown in the greenhouse at day/night temperature of 25/22 °C. The supplemental light simulated a 12 h photoperiod (7:00 to 19:00 h). Relative humidity (RH) was maintained at approximately 60% (every 15 min, spells of 1 min misting the air to increase RH). Eighteen days after sowing, the rice plants were divided into three groups receiving different mineral N application rates: low-N fertilizer (no supplementary mineral N fertilizer (0 mg Nmin/kg soil)), medium-N fertilizer (adding 75 mg Nmin/kg soil of ammonium-nitrate-N, corresponding to 125 kg N/ha), and high-N fertilizer (adding 150 mg Nmin/kg soil of ammonium-nitrate-N, corresponding to 250 kg N/ha). All treatments received NPKMg and trace elements in the form of NovaTec® Classic (COMPO EXPERT GmbH, Krefeld, Germany) four days before inoculation.

The experiment was carried out twice, with a total of 117 pots for each experiment. The pots were divided into three groups: (1) a set of 45 pots were used (three rice genotypes, three N treatments, and five replications (pots) per treatment) for the SPAD and total nitrogen (N) analysis; (2) 54 pots were used (three rice genotypes, three N treatments, three pathogen isolates, and two replications) for pathogen inoculation; (3) 18 pots were used (three rice genotypes, three N treatments, and two replications) for non-inoculated control plants.

As interactions between rice and *M. oryzae* are gene-for-gene-specific, three isolates were used for inoculating rice leaves, comprising isolate Guy 11 (supplied by Didier Tharreau, CIRAD, Montpellier, France), isolate Li1497 (obtained from BASF, Limburgerhof, Germany), and isolate TH6772 (provided by Ulrich Schaffrath, University of Aachen, Germany). All isolates were cultivated on rice leaf agar medium. Conidia were produced, and the inoculum prepared as described [31]. At the 4-leaf stage (22-day-old seedlings), rice plants were spray-inoculated with a *M. oryzae* conidia suspension (10^5 mL⁻¹), using a hand sprayer. Inoculated plants were kept in a dark moist incubation chamber at 25 °C and >95% of RH for 24 h, before being returned to the greenhouse. During the incubation period, healthy (non-inoculated) control plants were maintained at 25 °C and 60% RH. The experiment was performed two times.

2.2. Measurements of Leaf Chlorophyll and N Content

The relative chlorophyll content (leaf greenness) was estimated as a proxy for the leaf N content using a SPAD-502 m (Konica Minolta, Inc., Osaka, Japan) [36]. The SPAD values were determined from the three uppermost fully expanded leaves of each individual plant four days after mineral N application. Three composite SPAD readings were taken from the base, the middle, and the tip of each leaf. Five plants were measured from every pot and the SPAD readings were averaged to represent the mean value of each pot. Each

experiment consisted of 45 pots, whereby the average of 5 composite SPAD values was recorded separately for each genotype and each mineral N treatment ($n = 5$ replications).

After recording of SPAD values, the aboveground biomass of rice plants was obtained for the analysis of total N content, following oven drying at 70 °C for 72 h and subsequently mill-grinding (Wiley Mill, Thomas Scientific, Philadelphia, PA, USA). Total N content was analyzed by Duma's combustion method using a CNS elemental analyzer (Model: EUROEAP, EuroVector, Milan, Italy). The experimental unit for dry matter and N content was the biomass per pot ($n = 5$).

2.3. Measurement of Leaf Reflectance of Spectral Information

Hyperspectral images of healthy leaves were recorded 4 and 11 days after mineral N supply, and 7 days post inoculation (dpi) for diseased leaves. Spectral reflectance was obtained under controlled conditions in a dark room using an ImSpector V10E hyperspectral imaging system (Specim, Spectral Imaging Ltd., Oulu, Finland) at a spectral range of 400–1000 nm, and with 2.8 nm spectral resolution (212 wavebands). The line-scanning spectrograph capturing 1600 pixels per line was mounted on a stereo microscope foreoptic (Z6 APO, Leica, Wetzlar, Germany) equipped with an OLE-23 lens (Spectral Imaging Ltd., Oulu, Finland). Plant leaves were positioned on a XY-motorized table (H105/2/0 ProScan Upright Stage, Prior Scientific, Jena, Germany), which was moved below the optical system, resulting in the recording of spectral data cubes for imaging approaches. The working distance between leaf tissue and optical lens was 105 mm; a $3.6\times$ magnification resulted in a spatial resolution of 6.3 μm per pixel. Two linear line lights attached to a 150 W cold light source (Schott, Mainz, Germany) via a non-absorbing fiber (DCR[®] Light Source EKE, Polytec, Waldbronn, Germany) provided homogenous illumination. The instrument was warmed-up for 60 min before measurement were taken to maintain constant and reproducible illumination and constant sensitivity of the sensor unit.

For image recording, a single leaf attached to the rice plant was placed flat on the stage. Four hyperspectral images were taken for each sample, using the software Lumo Recorder[®] (Spectral Imaging Ltd., Oulu, Finland): (i) an image of the object area of interest with an optimized exposure time; (ii) a dark current image of the object; (iii) an image of a white reference bar (Zenith Polymer Target, SphereOptics GmbH., Uhldingen-Mühlhofen, Germany); and (iv) a dark current image of the white reference. In each mineral N treatment, spectra from four leaves per genotype were measured. A total of 72 leaf images (2 time steps \times 3 genotypes \times 3 N levels \times 4 replications) were analyzed for non-inoculated plants, and 108 leaves (3 \times 3 \times 3 \times 4 replicates) in inoculated plants.

2.4. Pre-Processing of Hyperspectral Images

Hyperspectral images were pre-processed using IDL 8.3/ENVI 5.3 software (ITT Visual Information Solutions, Boulder, CO, USA). The reflectance of hyperspectral images was calculated by normalizing the images relative to the reflection of the white reference and using the dark current image for signal correction. Because of a low signal-to-noise ratio at the extremes of spectra, only wavelengths between 450 and 850 nm (=140 wavebands) were used for analyses. The resultant spectral signals were smoothed using the Savitzky–Golay filter [37].

2.5. Analysis of Hyperspectral Data

For supervised classification of spectral information, the spectral angle mapper (SAM) algorithm was applied [38]. SAM calculates the spectral angle between the spectrum of each pixel and reference spectra from a spectral library by treating them as vectors in a dimensionality that equals the number of bands. The smaller the angle, the higher the similarity. SAM is relatively robust to changes in illumination conditions. As a supervised classification algorithm, SAM has the advantage that classes (=phenotypes/endmembers) to be included in the data analysis are predefined. Image pixels were categorized as belonging to the classes (=endmember) healthy (green) tissue or various blast symptom

subareas. A spectral library including reference spectra of the classes was created, using manually marked regions of interest (ROIs) for the different tissue types, i.e., healthy tissue, and dark brown, grey, chlorotic, grey green, and light brown tissues for subareas of blast symptoms at each level of mineral N supply. ROIs included >37,500 pixels for healthy tissue and ranged from 33 to >1000 pixels for blast symptom subareas. The mean spectrum of each ROI was stored as reference spectra in a spectral library and used for pixelwise SAM classification of hyperspectral images.

The SAM algorithm calculated spectral similarities of pixels of interest and all reference spectra selected in an n-dimensional space, depending on the number of spectral bands. The algorithm categorizes pixels by assigning them to the reference components or leaves them unclassified. Classification results are visualized in false-color images. Four leaves for each rice genotype \times *M. oryzae* interaction at low, medium, and high mineral N levels were analyzed. To investigate the effect of mineral N supply on the spectra of healthy tissue and blast symptom subareas, differences between spectra were calculated by subtracting the reflectance of leaves at low N supply from the reflectance of those at medium and high N supply for each wavelength. Peaks in difference spectra (Δ medium N – low N, and Δ high N – low N) indicated to wavelengths at which significant differences between mineral N application rates occurred.

The red edge inflection point (REIP) of spectra was calculated according to the equation:

$$\text{REIP} = 700 + 40 \left(\frac{(R_{670} + R_{780})/2 - R_{700}}{R_{740} - R_{700}} \right) \quad (1)$$

where R_{670} , R_{700} , R_{740} , and R_{780} represent reflectance values at 670, 700, 740, and 780 nm wavelengths, respectively [39].

2.6. Assessment of Blast Symptoms in RGB Images

In addition, RGB images of diseased leaves, taken with the HSI system were used for digital image analysis. The images were analyzed using the software Assess 2.0 (American Phytopathological Society, St. Paul, MN, USA) to determine the percentage of diseased leaf area, mean lesion area [mm^2], and the number of blast lesions per leaf area on the leaves of rice genotypes grown at low, medium, and high mineral N supply. In these experiments, leaf images were the experimental unit ($n = 4$).

2.7. Statistical Analysis

Standard analysis of variance (ANOVA) was applied to determine the significance of effects of mineral N supply on relative chlorophyll and total N content, disease severity (percentage leaf area diseased), blast lesion area, and on lesion number, using R studio version 4.2.1 statistical software [40]. Mean separation was performed by Tukey's HSD test at ($p = 0.05$). The number of replicates used for statistical analysis (n) is provided in the results. All experiments were performed two times. Despite minor differences in absolute values among experiments, biological repetitions confirmed a significant difference between treatments or the ranking of treatments.

3. Results

3.1. Rice Plant Response to Increased Mineral N Supply

The phenotypic response of the rice genotypes CO 39, IR64, and Nipponbare to low, medium, and high N supply was assessed 4 days after N fertilizer application (Figure S1). At a low N supply, plant height, and leaf size were smallest, and leaves showed symptoms of slight chlorosis. All genotypes responded to increasing N application by significantly ($p < 0.05$) enhancing leaf greenness, leaf size (Figure S1), and dry biomass (Figure S2). Similarly, across genotypes, mineral N supply significantly increased relative leaf chlorophyll content or leaf greenness by 47–56%, and total N contents from 1.8 (low) to over 4.0 (medium) to 4.5 (high) %N in the dry matter (Figure 1). In general, Nipponbare had significantly more leaf chlorophyll and higher total N than CO 39 and IR64, irrespective of the mineral N rate applied.

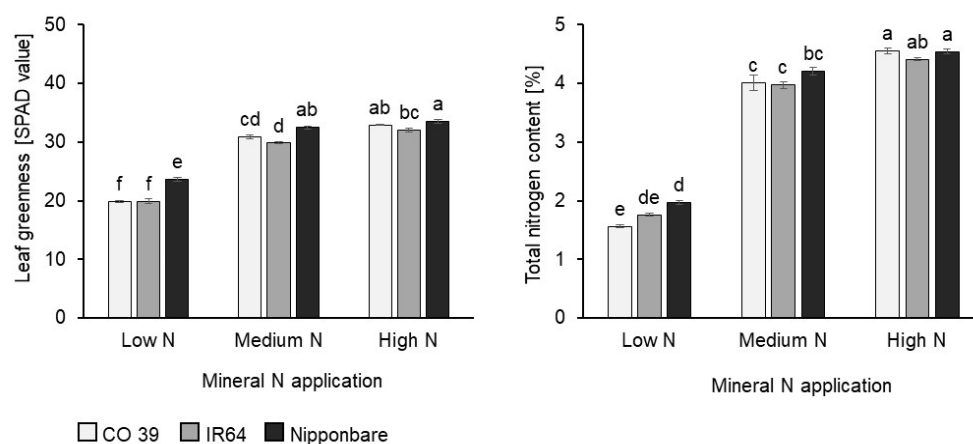


Figure 1. Effect of mineral N supply (low, medium, high) on leaf greenness (SPAD) and leaf N content of rice genotypes CO 39, IR64, and Nipponbare 4 days after N fertilizer application. Data represent the mean \pm standard error ($n = 4$). Letters from Compact Letter Display (CLD) denote statistically significant differences by Tukey's HSD test ($p = 0.05$).

3.2. Effect of Mineral N Supply on the Spectral Signature of Healthy Leaves

The spectral reflectance of non-inoculated rice leaves in the visible (VIS) and near-infrared (NIR) ranges was recorded at 4 and 11 days after mineral N application. The reflectance patterns were similar in healthy (non-inoculated) plants at all three mineral N supply rates (Figure 2). In the range 400–700 nm, mean reflectance signatures were higher at a low mineral N supply than at a medium and high mineral N supply. Differences between the medium and high N rates were moderate to low, irrespective of rice genotypes or time after mineral N supply (4 and 11 days, Figures 2a and 2b, respectively). Except in IR64 and Nipponbare that showed a reflectance decrease in the VIS at high N supply, reflectance in this spectral region increased with time after N supply (Figure 2), and it was consistently and significantly highest at a low N supply, regardless of the rice genotype. At medium N supply, significant differences between spectral signatures appeared only 11 days after N supply, while minor differences in the spectral reflectance were already apparent 4 days after N application at high N application rates. Genotypes CO 39 and IR64 reacted similarly to mineral N supply and were significantly different from Nipponbare (Figure S3). Similarly, mineral N application differentially affected the REIP and the reflectance in the NIR range (780–800 nm) of the spectrum. Increased mineral N supply caused a decrease in the green peak, while increasing the reflectance in the NIR range, and showed a shift in REIP to longer wavelengths (Figure 2).

Difference spectra also revealed significant differences among leaves of genotypes grown under different N supply (Figure 3). In the range of the green peak and the red edge, spectral differences between high and low mineral N supply were significant for all genotypes. While the spectra of CO 39 did not differ in the visible and the red-edge regions at 4 days, spectral differences between N rates were significant for all genotypes 11 days after N application. However, spectra in the NIR range differed as early as 4 days after mineral N application in all genotypes. While being less pronounced, the reflectance spectra in the NIR range increased more at high than at moderate N supply. The effect of mineral N on the reflectance of healthy leaf tissue was strongest in IR64 and weakest in Nipponbare, while CO 39 showed an intermediate response (Figure 3). Between 4 and 11 days after N application, leaf reflectance in the VIS range increased with a low N supply and decreased with a high N supply. At medium N supply, IR64 and Nipponbare showed intermediate reflectance patterns, while in CO 39, the genotype with the highest biomass, reflectance consistently increased with the N rate. The strongest time effects (changes from 0 over 4 to 11 days after N application) were observed in IR64, indicating significant interactions between N rates and time (Figure S4).

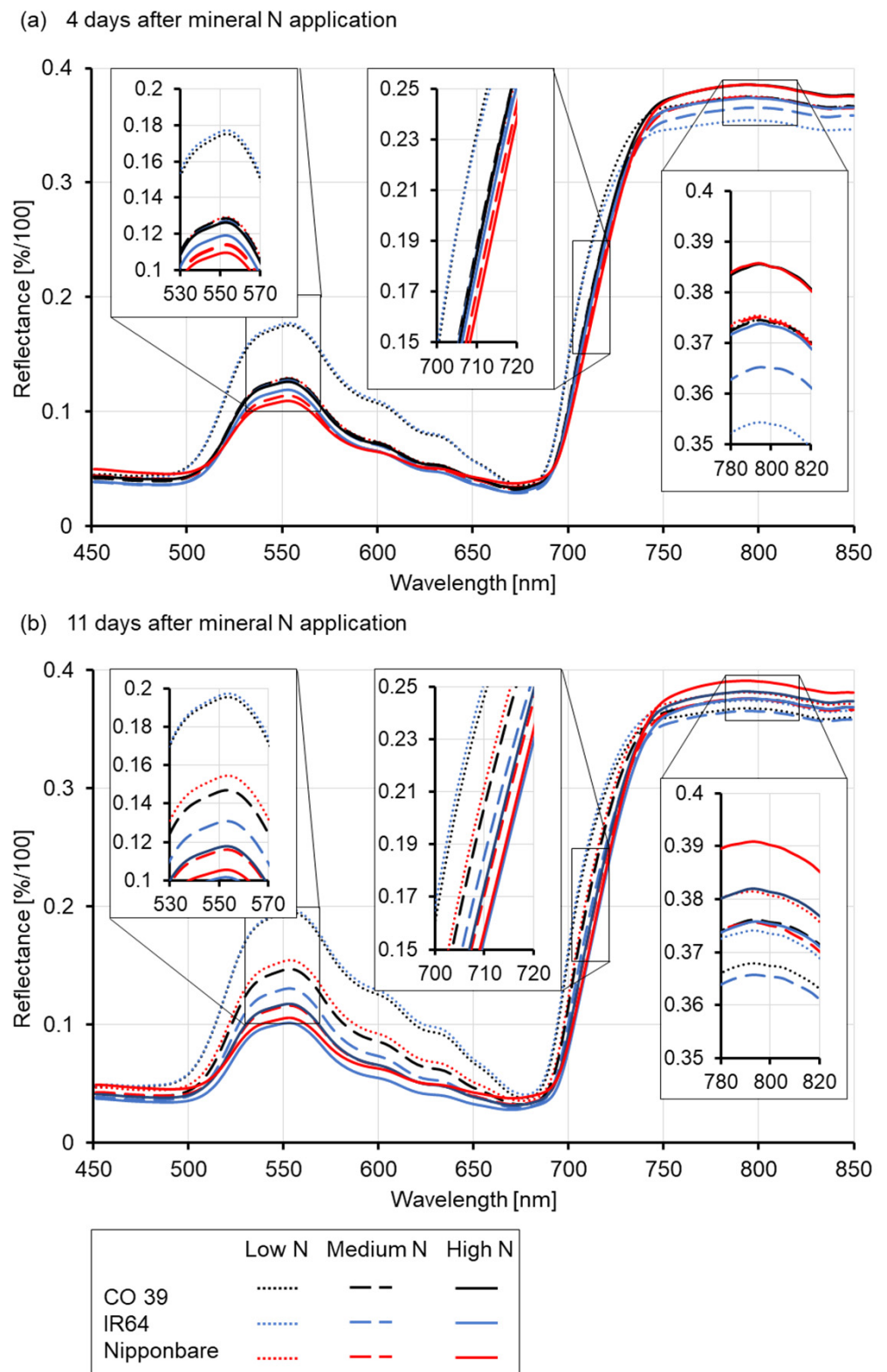


Figure 2. Effect of mineral N supply (low, medium, high) on the reflectance of healthy leaves of three rice genotypes. Average reflectance spectra of rice genotypes CO 39, IR64, and Nipponbare at (a) 4 and (b) 11 days after N fertilizer application. Scaled-up inserts highlight the spectral ranges showing the most prominent changes.

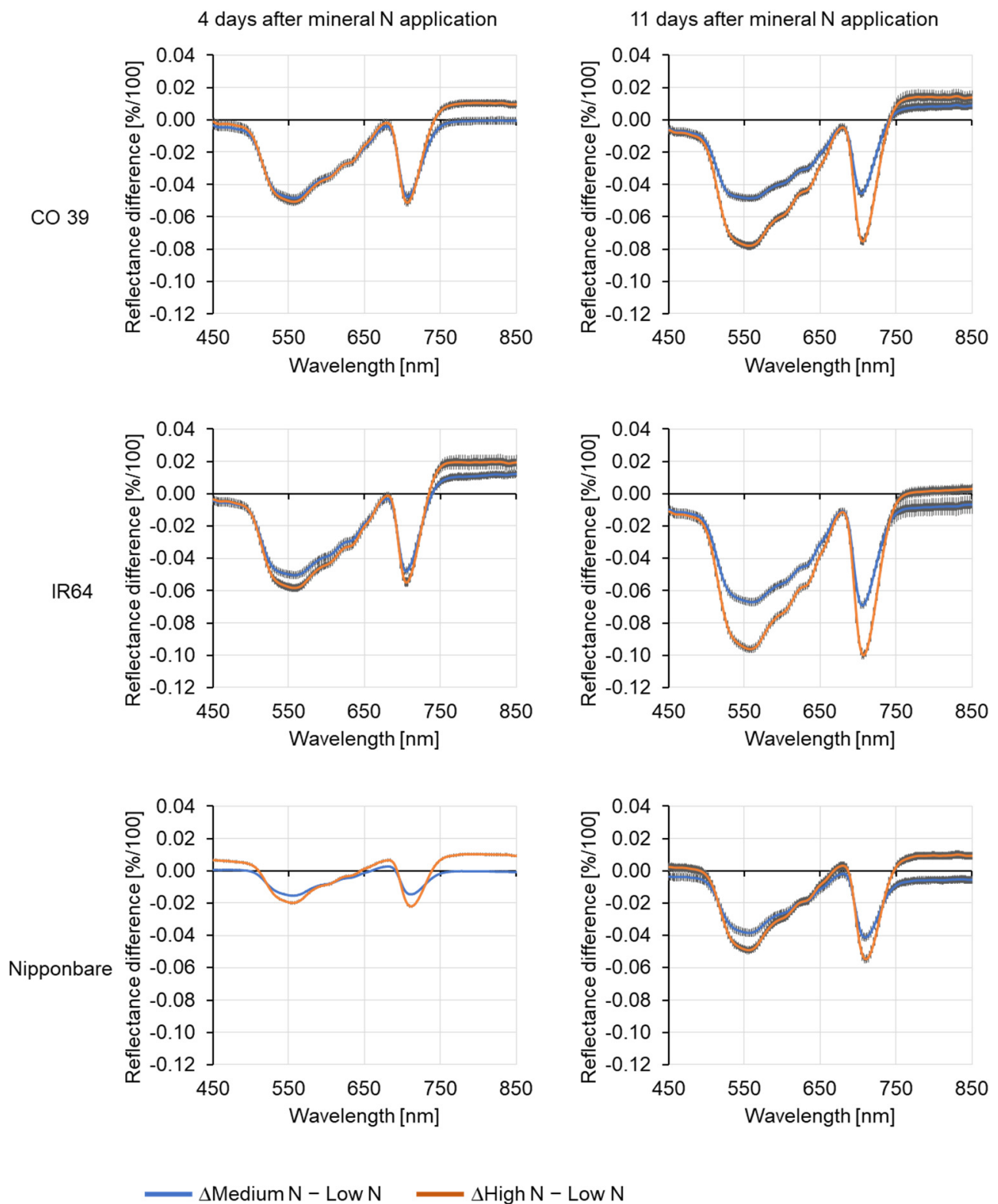


Figure 3. Difference spectra of reflectance of healthy leaf tissue of rice genotypes CO 39, IR64, and Nipponbare grown at low, medium, and high N supply 4 and 11 days after N fertilizer application. The zero line displays the reflectance of plants grown at low N supply as a reference. For each waveband, the bars represent the standard error of the mean ($n = 4$).

3.3. Effects of Mineral N Supply on the Expression of Leaf Blast Symptoms

The reaction of rice genotypes grown at low, medium, and high mineral N supply to infection by *M. oryzae* was assessed 7 days post inoculation (=11 days after mineral N supply; Figure 4). The number, size, and intensity of leaf blast symptoms varied depending on the interaction among rice genotypes, *M. oryzae* isolates, and rates of mineral N supply, indicating gene-for-gene-specific and N × cultivar interactions. Genotype IR64, infected by *M. oryzae* isolates Guy 11, Li1497, and TH6772, retained its blast resistance at all N application rates. On the other hand, rice genotype CO 39, moderately resistant to isolate TH6772, showed less and smaller dark-brown spots at a low N supply than at a medium and high N supply (Figure 4). Characteristic blast lesions in Nipponbare consisted of a grey tissue surrounded by a dark-green border, with chlorotic areas and brown tissue at the margins. The symptoms associated with isolates Guy 11 and Li1497 on the blast-susceptible rice genotype CO 39 ranged from dark brown areas to white or grey centers, surrounded by grey green tissue. The size of these lesions tended to increase with mineral N supply (Figure 4).

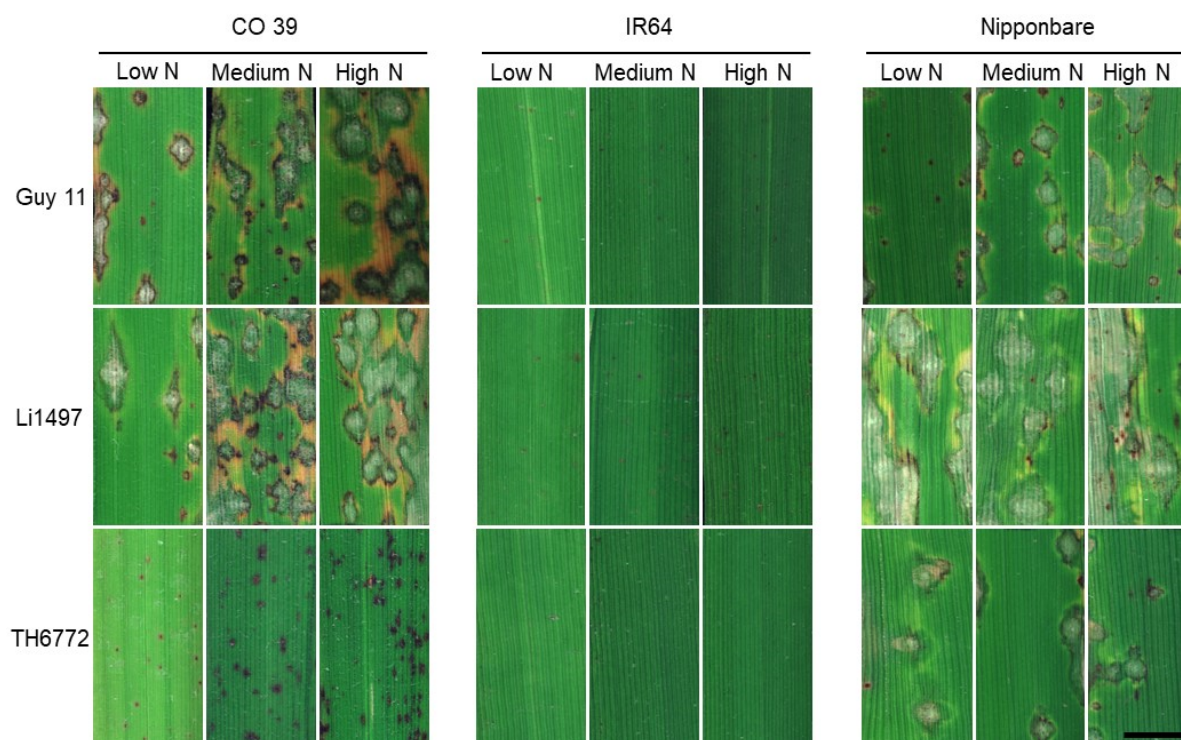


Figure 4. Phenotypes of representative leaf blast symptoms on rice genotypes CO 39, IR64, and Nipponbare infected by *M. oryzae* isolates Guy 11, Li1497, and TH6772 at low, medium, and high N supply, respectively. Images were taken 7 days post inoculation corresponding to 11 days after N fertilizer application (bar size = 5 mm).

3.4. Effects of Mineral N Supply on Rice Blast Intensity

The number and the size of blast lesions as well as the percentage of diseased leaf area 7 days post inoculation depended on the mineral N supply. The number of lesions was lowest at low mineral N supply, irrespective of the host–pathogen genotypes involved (Figure 5, top row). However, with increasing N supply, the number of blast lesions increased significantly ($p < 0.05$) in rice genotypes CO 39 and Nipponbare, inoculated with isolate TH6772. Lesion numbers in resistant interactions were often higher than in highly susceptible interactions. Apart from the number of lesions, lesion sizes also differed among rice genotypes, *M. oryzae* isolates, and mineral N application rates. The mean size of blast lesions was very small in resistant interactions and was not significantly affected

by N supply. The lesion size in susceptible interactions tended to increase with mineral N supply (Figure 5, middle row). In the Nipponbare \times Li1497 combination, lesion size in low and high N was higher than in medium N; however, the differences were not significant ($p < 0.05$). In the Nipponbare \times TH6772 interaction, lesion sizes in low N tended to be higher than in medium and high N. Depending on the specific combination of host, pathogen, and mineral N level, rice leaves at low N supply exhibited N depletion earlier at the site of pathogen infection and consequently disease lesions developed faster than in plants under medium and high N supply.

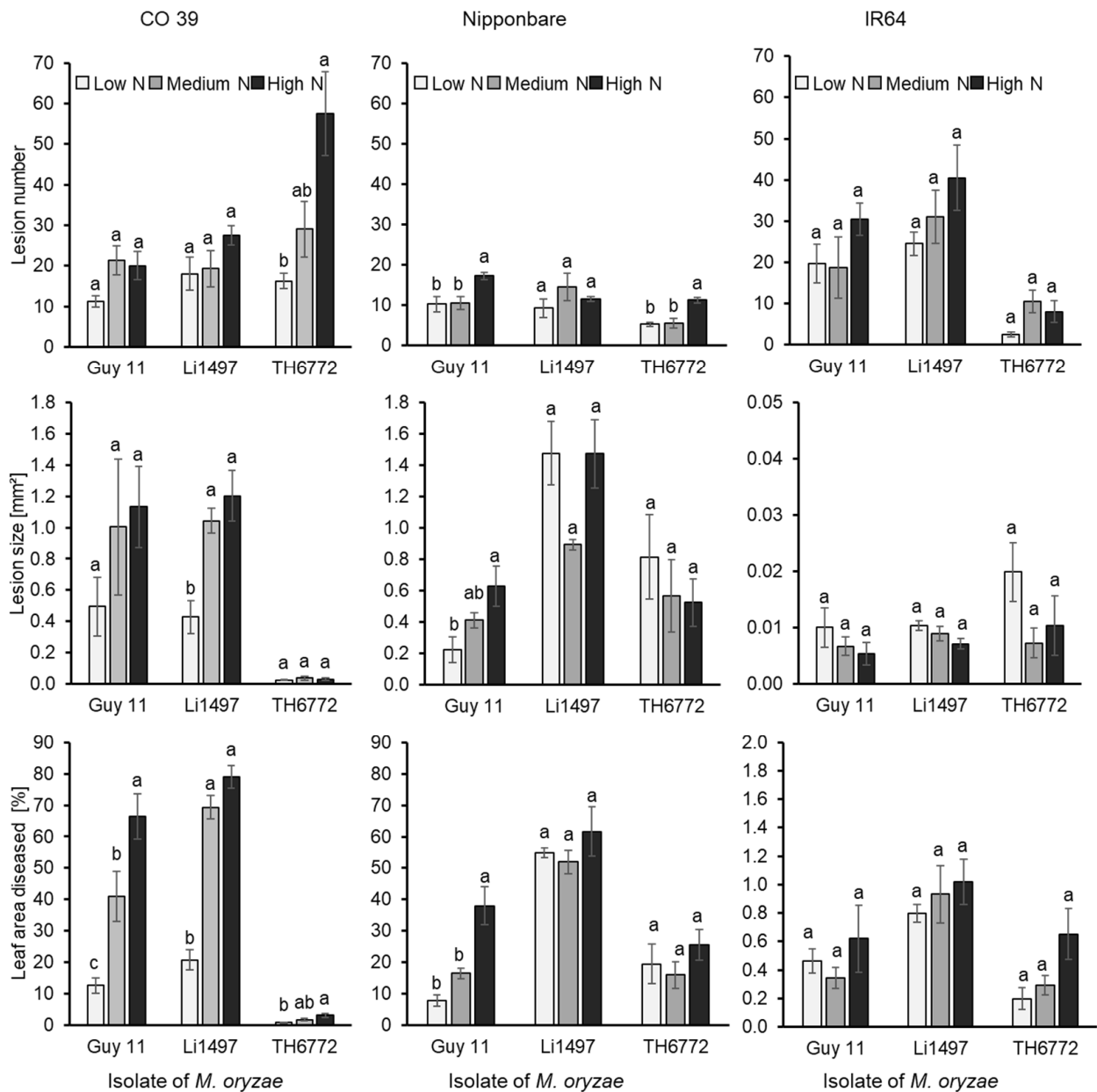


Figure 5. Effect of low, medium, and high mineral N supply on the number of blast lesions, mean lesion area, and disease severity due to infection of three rice genotypes CO 39, IR64, and Nipponbare by three isolates of *M. oryzae* Guy 11, Li1497, and TH6772. Number of blast lesions/leaf area [mm²], mean area of blast lesions [mm²], and leaf area covered by blast symptoms [%] were measured 7 days post inoculation. Data represent the mean \pm standard error ($n = 4$). Bars annotated by the same letter from Compact Letter Display (CLD) do not differ significantly according to Tukey's HSD test ($p = 0.05$).

The percentage of diseased leaf area was the parameter most suitable to measure the effect of mineral N on leaf blast intensity. In genotype Nipponbare, infected with isolates Li1497 and TH6772, respectively, disease severity at low and high N was higher than at medium N; however, differences in blast severity were not significant ($p < 0.05$) as plants were susceptible at all N levels. Similarly, the higher blast severity at low and high N in genotype IR64 infected with Guy 11 was not significantly ($p < 0.05$) different from the severity at medium N level. In all other combinations of host genotypes and pathogen isolates, the leaf blast intensity was lowest at low N supply, and it increased with N application rates (Figure 5, bottom row). Differences between high and low N supplies were significant ($p < 0.05$) in susceptible interactions, with no significant effects on blast intensity in the case of incompatible interactions (i.e., IR64 \times all isolates). In the moderately resistant interaction CO 39 \times TH6772, leaf blast increased with N supply, albeit at an overall low disease level.

3.5. Effect of Mineral N Supply on Leaf Blast Symptom Types of Rice Genotypes

The SAM algorithm was used for the supervised classification of blast symptom types on leaves of the three rice genotypes grown at low, medium, and high N supply (Figure 6). Irrespective of N rates, the susceptible genotypes CO 39 and Nipponbare were characterized by more complex blast symptoms, resulting in five symptom subareas: (1) dark brown tissue, (2) grey tissue, (3) chlorotic tissue, (4) grey green tissue, and (5) light brown tissue. In the resistant genotype IR64, only small dark brown leaf spots were observed, irrespective of the mineral N rates applied. The number of tissue types varied with the compatibility of the host–pathogen interaction and mineral N supply rate.

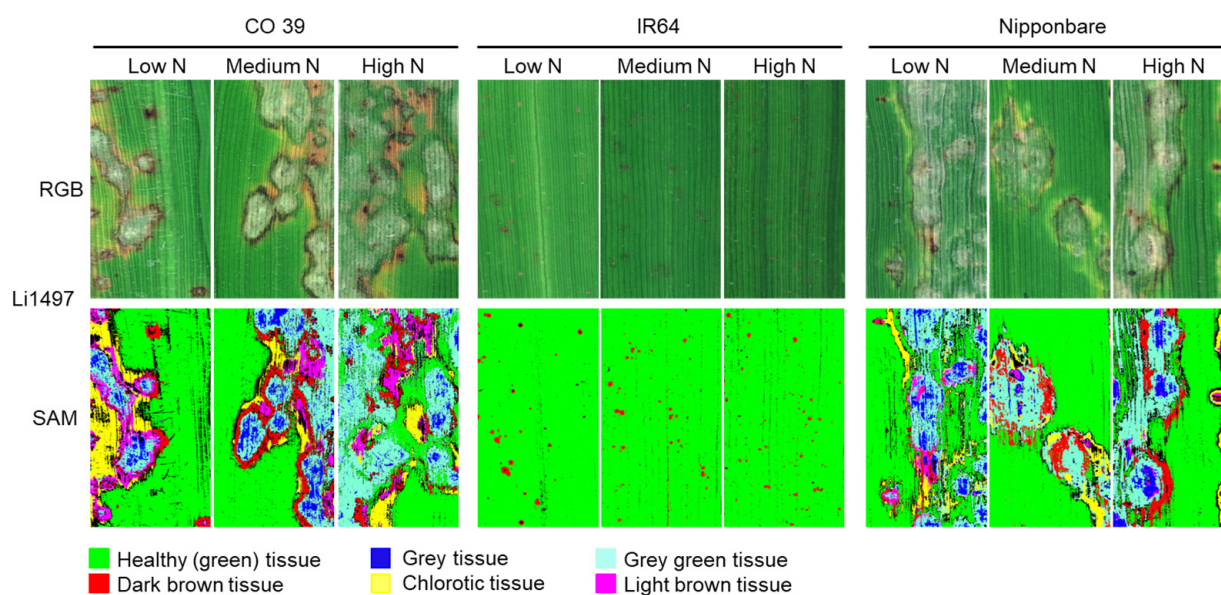


Figure 6. Classification of blast symptom subareas on leaves of three rice genotypes CO 39, IR64, and Nipponbare inoculated with *M. oryzae* isolate Li1497 at low, medium, and high mineral N supply. Images were recorded 7 days post inoculation. RGB images of the different tissue reactions were used as ground truth. Healthy green tissue and different subareas of blast symptom types were classified in supervised classification by spectral angle mapper (SAM) algorithm. For genotype IR64 (resistant), small dark brown leaf spots were classified, while for genotypes CO 39 (highly susceptible) and Nipponbare (susceptible), blast symptom subareas included dark brown tissue, grey tissue, chlorotic tissue, grey green tissue, and light brown tissue.

3.6. Variability of Spectral Signatures of Blast Symptom Types as Affected by Mineral N Supply

From the interactions between rice genotypes CO 39, IR64, Nipponbare, and *M. oryzae* isolates Guy 11, Li1497, and TH6772, respectively, representative spectra of healthy green

tissue and subareas of blast symptom were analyzed 7 days post inoculation. The reflectance of leaf tissue was affected by both mineral N supply and blast symptom subareas as shown for the interaction between rice genotypes and *M. oryzae* isolate Li1497 (Figure 7). For healthy tissues, the spectral reflectance of the green peak decreased with increasing N supply in genotype IR64 and was unaffected in the other genotypes. In the compatible interaction between genotypes CO 39 and Nipponbare the spectral reflectance of grey blast symptom subareas were consistently higher than that of healthy tissues. While the spectral reflectance of grey green and chlorotic tissues (exclusively occurring in compatible rice—*M. oryzae* interactions) increased in the VIS region, the reflectance of dark brown tissues (representative for resistance reactions to pathogen infection) decreased in the VIS and NIR regions of the spectrum compared to healthy tissues (Figure 7).

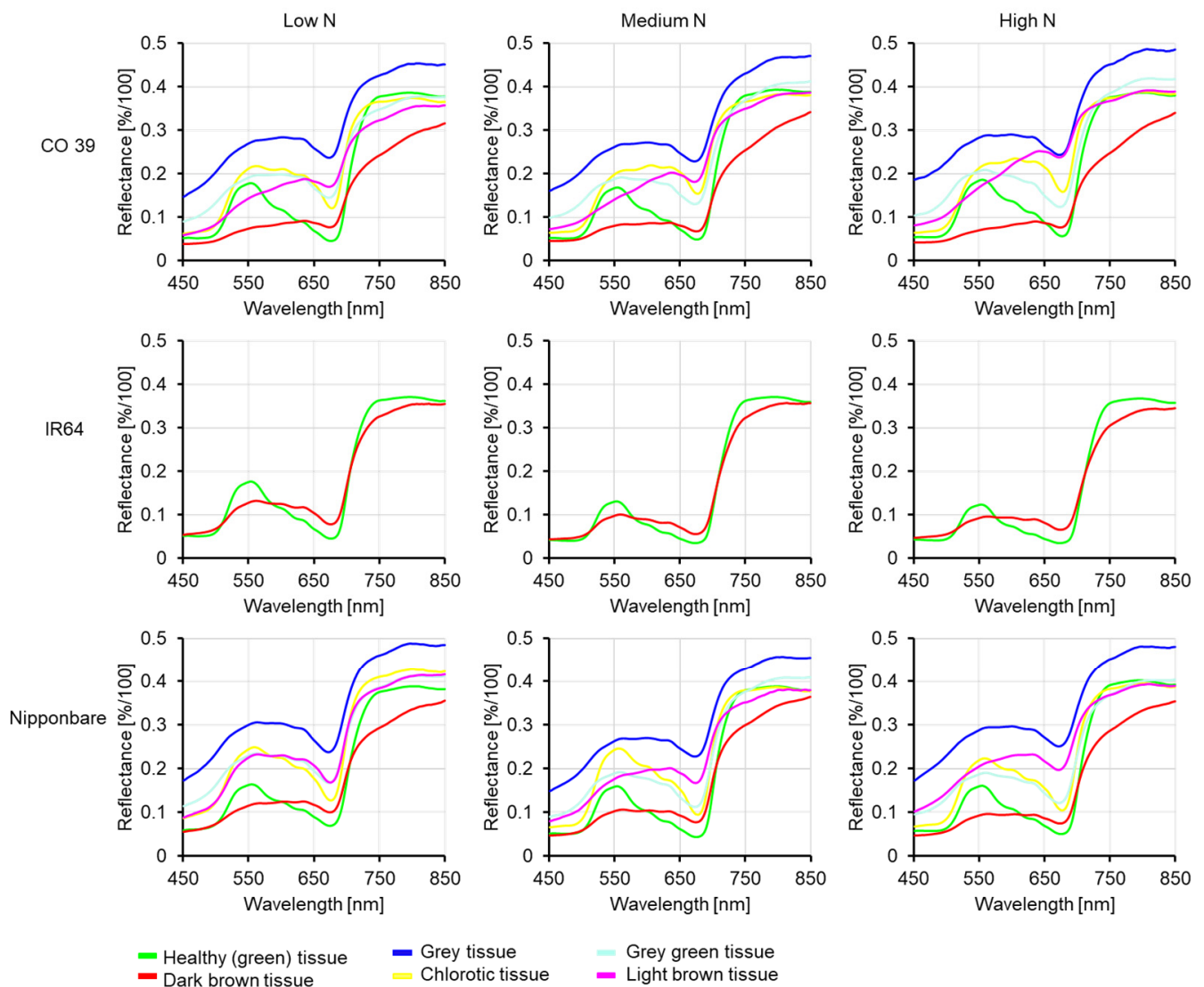


Figure 7. Mean spectral signatures of healthy green tissue and various blast symptom subareas of the three rice genotypes CO 39, IR64, and Nipponbare inoculated with *M. oryzae* isolate Li1497 at low, medium, and high mineral N supply, respectively, 7 days post inoculation.

The effects of N supply on reflectance signatures were further investigated by calculating reflectance differences between medium and low N supplies, and between high and low N supplies. In the susceptible interaction CO 39 \times Li1497, mineral N supply affected the spectrum of dark brown tissues. In Nipponbare and the resistant genotype IR64, increasing

the N supply reduced the reflectance of dark brown tissues in the green and red range of the spectrum. The grey tissue type, representing leaf tissue with highest reflectance values, reacted differently to mineral N supply. Thus, high mineral N significantly affected reflectance in the blue range of susceptible genotype CO 39, and in the blue and green ranges of moderately susceptible genotype Nipponbare. The effect of mineral N supply on spectral characteristics of grey green tissues differed between genotypes CO 39 and Nipponbare. Thus, CO 39 showed a significant effect in the green, red edge, and NIR ranges, while in Nipponbare, the reflectance was significantly reduced in the VIS range (Figure 8). In general, each rice genotype reacted differently to increasing N supply, revealing genotype-specific response patterns (Figure 9a–f). Consequently, genotype-specific responses to blast infection and mineral N supply can be differentiated by their distinct spectral signatures, permitting tissue-type-specific differentiations of susceptible and resistance blast response patterns.

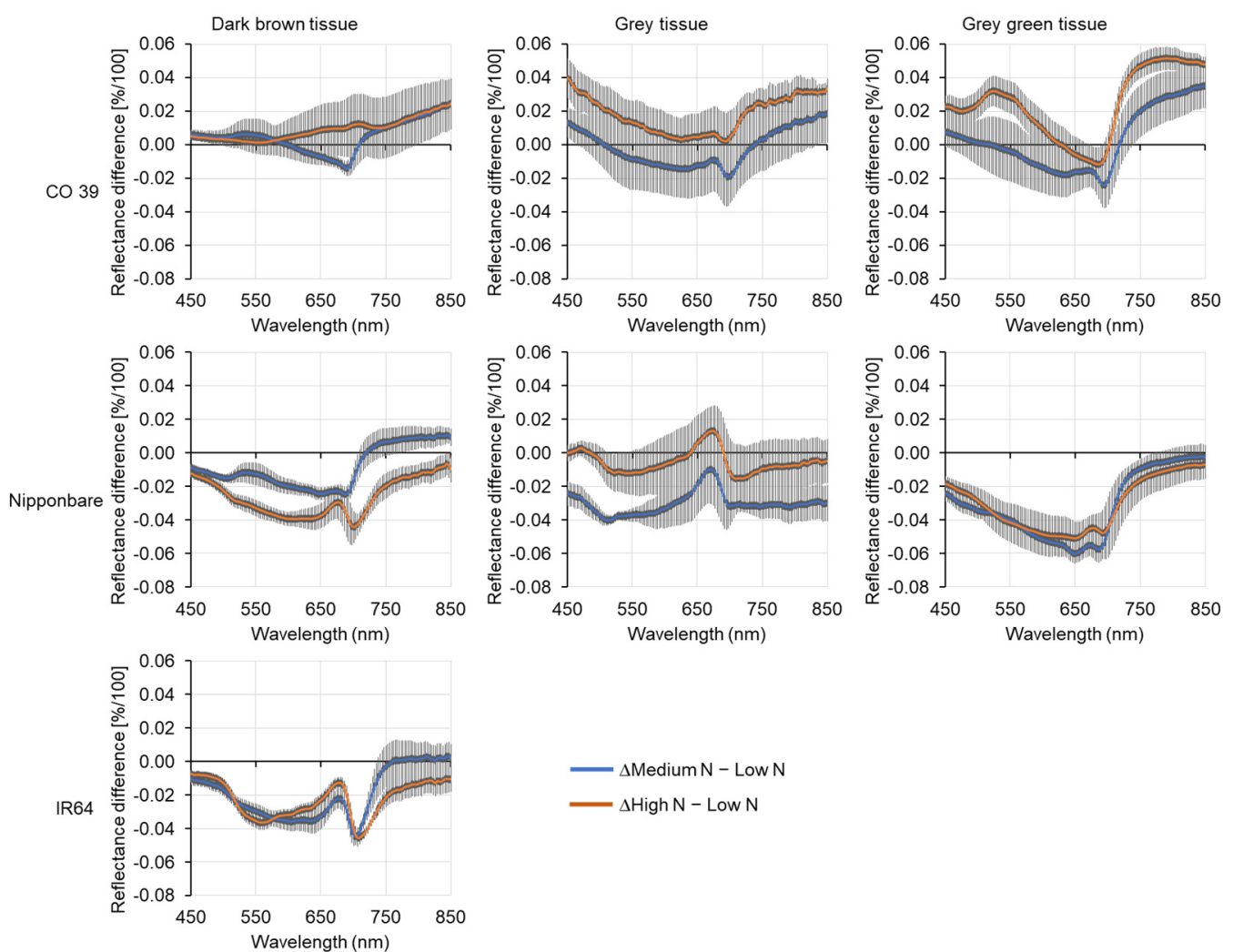


Figure 8. Difference spectra of blast symptom subareas of rice genotypes CO 39, IR64, and Nipponbare infected by *M. oryzae* isolate Li1497 at low, medium, and high mineral N supply, respectively. Differences were computed by subtracting the reflectance of blast symptom subareas from diseased leaves at low N supply from corresponding subareas from leaves at medium and high N supply, respectively. The baseline reflects the average reflectance of symptom subareas from leaves at low N supply. Bars represent the standard error of the mean for each waveband ($n = 4$).

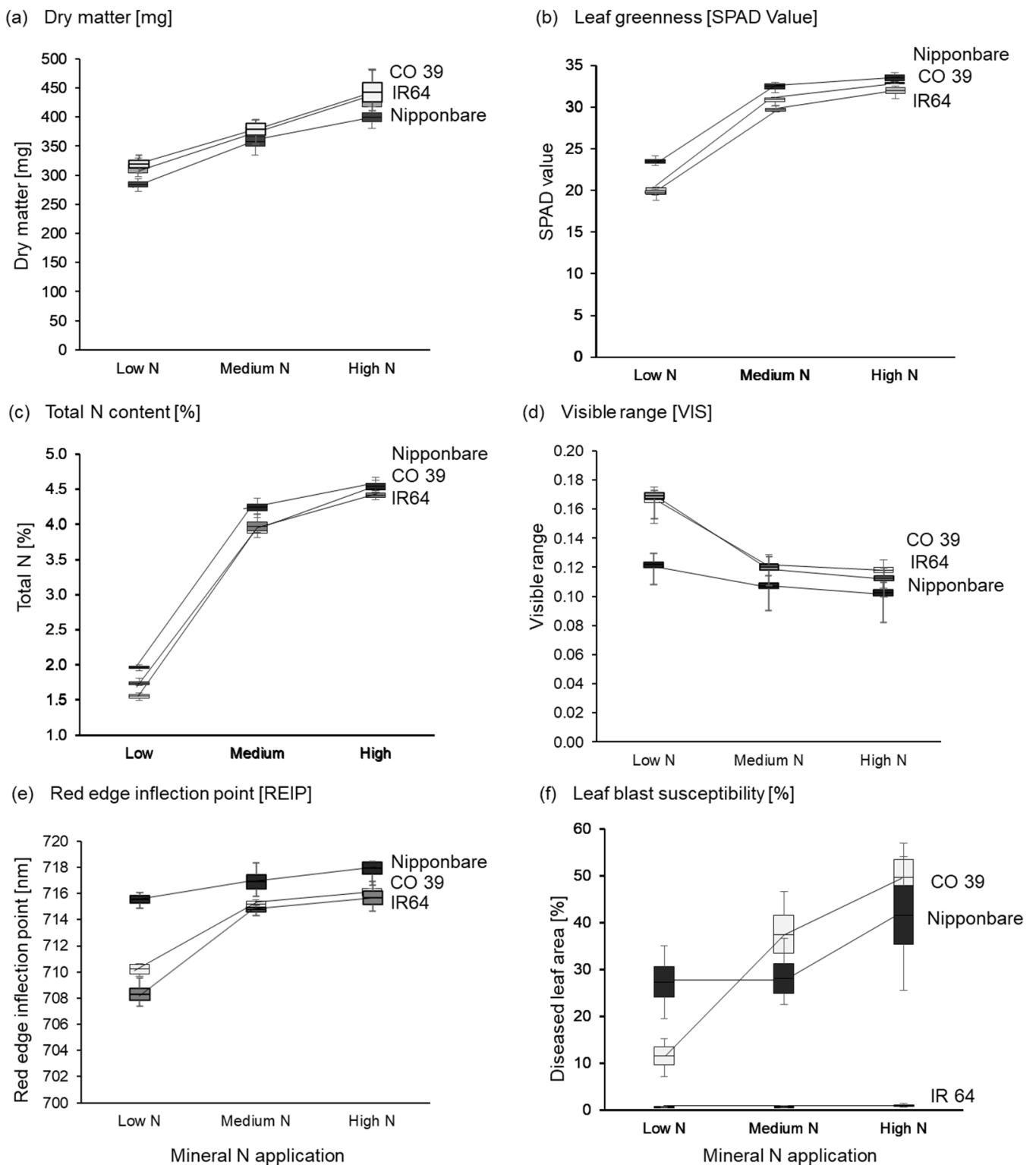


Figure 9. Genotype-specific differences among rice genotypes CO 39, IR64, and Nipponbare for (a) dry matter content [mg], (b) leaf greenness, (c) total N content [%], (d) visible range, (e) the red edge inflection point, and (f) disease severity [%], at low, medium, and high mineral N supply. The boxes denote the mean as well as the standard error of the mean; whiskers represent the minimum and maximum values ($n = 4$).

4. Discussion

The present study confirms the reported literature data, showing that mineral N supply to rice is associated with increased plant growth and leaf greenness [41,42], and a near-doubling of the leaf N content [43,44], albeit while increasing rice plants' susceptibility to leaf blast. Both rice performance attributes and the type and severity of blast symptoms related to mineral N supply were differentiated by their spectral signatures.

Mineral N supply increases the leaf chlorophyll content, and a photometer-based sensing of the leaf greenness is used as a proxy for determining leaf N concentrations. The N-induced decrease in leaf reflectance in the VIS and red-edge ranges is the result of absorption of irradiance by chlorophyll [25]. These relationships are used for guiding site-specific N management in maize [45], wheat [4], and rice [46]. In the present study, mineral N supply affected the spectral characteristics of rice leaves only 4 days after N application. However, the extent of the spectral responses differed by rice genotype. For two out of three rice genotypes, the effect of mineral N supply on spectral characteristics and total N content of leaves was stronger for the increase from low to medium N than for the increase from medium to high N supply. Such differences are related to anatomical and to physiological attributes of rice. Consequently the leaf thickness (or specific leaf weight), is recommended to be used as a correction factor for guiding site-specific (photometer-based) N management in rice [46]. Additionally, attributes in N use efficiency traits may reportedly account for genotype-specific differences in spectral responses of upland rice [41]. Such interactions between genotypes and mineral N supply rates, and their effects on the leaf greenness, require genotype-specific adjustments of photometer readings. This complicates the interpretation of reflectance data and may hamper the extrapolation of findings to very diverse sets of rice genotypes.

The observed shift in REIP appears to be the most robust indicator of mineral N supply. Being sensitive to small differences in the plant's N status, this parameter appears most suitable for optimizing the N supply to rice plants. Changes in NIR reflectance were less consistent, which is reportedly associated with scattering of NIR wavelengths [23]. This result is also consistent with other recent studies, using non-imaging hyperspectral systems [47,48].

While increased N availability improves plant performance attributes, it may also increase the rice plants' susceptibility to fungal pathogens. Thus, high mineral N supply reportedly increases the severity of rice blast [9], wheat blast [49], and wheat stripe rust [4]. In the present study, high N supply generally increased the intensity of the rice blast disease similarly to earlier reports [9,50,51]. High mineral N supply thus increases the content of amino acids in rice leaf tissues and can serve as a substrate for the growth of pathogen [6]. In addition, elevated concentrations of nitrate in the vacuoles have been suggested to act as an N source for *M. oryzae*, increasing the susceptibility of tissues to the blast disease [52]. On the other hand, in some instances N-limited conditions can also trigger *M. oryzae* to induce its pathogenicity genes [53], and the *MPG1* gene has been highly expressed during appressorium formation and blast infection under N starvation *in vitro* [11].

However, such trade-offs of increased N fertilizer use on the occurrence of blast disease symptoms depend on rice genotypes and their interactions with different *M. oryzae* isolates [9,51]. In our study, the effect of mineral N supply on the development of leaf blast symptoms varied among rice—*M. oryzae* interactions, revealing gene-for-gene-specific interactions. While mineral N supply increased blast severity in the highly susceptible genotype CO 39 infected by *M. oryzae* isolate Li1497, it had no effect in the resistant genotype IR64, irrespective of the blast isolate. In rice genotype CO 39, infected by isolate Guy 11, mineral N supply increased blast severity by 25%, while the susceptibility of genotype Nipponbare to the same isolate increased only at the highest N rates. On the other hand, a high blast severity was observed in N-starved genotype Nipponbare when infected by *M. oryzae* isolate Li1497. Limited N availability *in planta* may thus stimulate pathogen growth and infection in blast-susceptible genotypes or genotypes × isolate combinations,

while high N availability does not affect the compatibility of host–pathogen interactions with the blast-resistant rice genotype.

The effects of a fungal disease on spectral signatures of leaf tissues depend on the type and intensity of biochemical and physiological changes in processes associated with infection and on the composition of disease symptoms [28,54]. The present study demonstrates that beyond fungal infection, the N status of plants affects reflectance patterns of diseased leaves and of different subareas of disease symptoms.

Leaf lesions are associated with the degradation of chlorophyll, which absorbs irradiance in the VIS range [29]. Similarly, cucumber leaves infected with angular spot disease increased the reflectance in the VIS region due to reduced leaf chlorophyll contents [33]. On the other hand, decreased VIS reflectance of dark brown spots results from light absorption by non-photosynthetic brown pigments [23]. The present study additionally showed that grey blast subareas were characterized by increased reflectance in the VIS and NIR regions, while grey green subareas and chlorotic tissues were characterized by either an increase or decrease in reflectance spectra in the NIR range, depending on the rice genotype and the N status of the leaf. A decrease in the reflectance spectra of dark brown tissues in the NIR range has been previously linked to the structural damage of rice tissue caused by the growth of *M. oryzae* within the leaf [29].

The spectral signature of blast symptom subareas demonstrated strong interactions with the N status of leaves; the largest spectral differences were observed in the VIS and red-edge ranges. The leaf N status increased or decreased spectral characteristics of symptom subareas, which significantly differed among rice genotype \times *M. oryzae* \times N supply rate interactions. As small spectral differences in reflectance of dark brown, grey, and grey green subareas of blast lesions could not be detected visually, HSI allowed for a more detailed analysis of the optical properties of diseased rice leaves.

Hyperspectral imaging at the microscopic level revealed high spatial and spectral variabilities in plant \times pathogen \times mineral N interactions at the leaf scale. Basic laboratory research benefits from the high spatial resolution and provides valuable insights into biophysical and biochemical changes caused by combined effects of both biotic and abiotic stressors. However, high labor requirements and a low throughput/small field of view limit the applicability of this approach in phenotyping and for field applications. In addition, the rice genotype \times *M. oryzae* \times N supply interactions resulted in a large diversity of blast subareas, hampering the establishment of a general library of reference spectra required in phenotyping platforms for quantitative blast resistance screening.

Proximal hyperspectral technologies at canopy scales may enable the establishment of a connection between leaf-level observations and large-scale measurements [55] and to upscale methods of canopy reflectance that were developed under controlled environments to field-scale studies [56]. Nevertheless, an increase in the HSI platform level is critical for the detection and characterization of small disease symptoms and low disease severities—in contrast to the assessment of abiotic effects on crops. Spectral differences at larger scales may be used for disease detection and for characterizing the crop's N status, provided the user accepts a coarse resolution of detecting the disease level. More detailed resolution data will require combining remote sensing, ground-truthing, and additional monitoring of environmental conditions. The more data available, the more reliable and detailed will be the information extracted from reflectance data.

5. Conclusions

Hyperspectral imaging at the microscopic level proved to be an effective tool for evaluating the effects of N supply on the spectral characteristics of healthy rice leaves, as well as on the variability of leaf blast symptoms, depending on gene-for-gene-specific host–pathogen interactions. Combining HSI with supervised classification by SAM could be adapted to a pixel-wise characterization of blast symptoms that differ in size and subarea attributes. Multiple interactions between plant genotypes, the level of N supply, and pathogen isolates result in large spectral variations, which complicate the interpretation

of spectral data. In phenotyping for breeding under (semi-)controlled conditions, spectral information may be used for identifying sources for disease resistance. However, the sensitivity and reliability of the sensor system will depend on its spatial resolution and on the variability of disease symptoms. A desired future application in remote sensing at the field level requires more data on factors affecting crop reflectance.

Supplementary Materials: The following supporting information can be downloaded at: <https://www.mdpi.com/article/10.3390/rs16060939/s1>, Figure S1: Characteristics of rice plants—genotypes CO 39, IR64, and Nipponbare—in response to increasing N levels 4 days after mineral N application. Figure S2: Effect of mineral N supply on total dry biomass of rice genotypes CO 39, IR64, and Nipponbare 4 days after N application. Figure S3: Effect of genotype on the reflectance of healthy rice leaves. Figure S4: Difference spectra of reflectance of healthy leaf tissue of rice genotypes CO 39, IR64, and Nipponbare grown at low, medium, and high mineral N supply.

Author Contributions: A.W.M., E.-C.O. and M.B. designed the experiment. A.W.M. performed the experiments; she carried out the hyperspectral measurements, analyzed the data, and drafted the manuscript. All authors have read and agreed to the published version of the manuscript.

Funding: This research was funded by a Ph.D. scholarship of the first author from Deutscher Akademischer Austauschdienst (DAAD) during the study.

Data Availability Statement: The original contributions presented in the study are included in the article/Supplementary Materials, and further inquiries can be directed to the first author.

Acknowledgments: The authors express their gratitude to Michael Frei, Department for Plant Nutrition, University of Bonn, Ulrich Schaffrath, RWTH Aachen (Germany), and BASF SE (Limburgerhof, Germany) for providing the rice genotypes used in the study. The authors also extend their appreciation to U. Schaffrath, Didier Tharreau (Montpellier, France), and BASF SE for the provision of *M. oryzae* isolates.

Conflicts of Interest: The authors declare that they have no conflicts of interest.

References

1. Makino, A. Photosynthesis, grain yield, and nitrogen utilization in rice and wheat. *Plant Physiol.* **2011**, *155*, 125–129. [[CrossRef](#)] [[PubMed](#)]
2. Dordas, C. Role of nutrients in controlling plant diseases in sustainable agriculture. A review. *Agron. Sustain. Dev.* **2008**, *28*, 33–46. [[CrossRef](#)]
3. Veresoglou, S.D.; Barto, E.K.; Meneses, G.; Rillig, M.C. Fertilization affects severity of disease caused by fungal plant pathogens. *Plant Pathol.* **2013**, *62*, 961–969. [[CrossRef](#)]
4. Devadas, R.; Simpfendorfer, S.; Backhouse, D.; Lamb, D.W. Effect of stripe rust on the yield response of wheat to nitrogen. *Crop J.* **2014**, *2*, 201–206. [[CrossRef](#)]
5. Walters, D.R.; Bingham, I.J. Influence of nutrition on disease development caused by fungal pathogens: Implications for plant disease control. *Ann. Appl. Biol.* **2007**, *151*, 307–324. [[CrossRef](#)]
6. Long, D.H.; Lee, F.N.; TeBeest, D.O. Effect of nitrogen fertilization on disease progress of rice blast on susceptible and resistant cultivars. *Plant Dis.* **2000**, *84*, 403–409. [[CrossRef](#)]
7. Wilson, R.A.; Talbot, N.J. Under pressure: Investigating the biology of plant infection by *Magnaporthe oryzae*. *Nat. Rev. Microbiol.* **2009**, *7*, 185–195. [[CrossRef](#)]
8. Mukherjee, A.K.; Mohapatra, N.K.; Suriya Rao, A.V.; Nayak, P. Effect of nitrogen fertilization on the expression of slow-blasting resistance in rice. *J. Agric. Sci.* **2005**, *143*, 385–393. [[CrossRef](#)]
9. Huang, H.; Nguyen Thi Thu, T.; He, X.; Gravot, A.; Bernillon, S.; Ballini, E.; Morel, J.-B. Increase of fungal pathogenicity and role of plant glutamine in nitrogen-induced susceptibility (NIS) to rice blast. *Front. Plant Sci.* **2017**, *8*, 265. [[CrossRef](#)] [[PubMed](#)]
10. Sun, Y.; Wang, M.; Mur, L.A.J.; Shen, Q.; Guo, S. Unravelling the roles of nitrogen nutrition in plant disease defences. *Int. J. Mol. Sci.* **2020**, *21*, 572. [[CrossRef](#)] [[PubMed](#)]
11. Talbot, N.J.; Ebbole, D.J.; Hamer, J.E. Identification and characterization of *MPG1*, a gene involved in pathogenicity from the rice blast fungus *Magnaporthe grisea*. *Plant Cell* **1993**, *5*, 1575–1590.
12. Muñoz-Huerta, R.; Guevara-Gonzalez, R.; Contreras-Medina, L.; Torres-Pacheco, I.; Prado-Olivarez, J.; Ocampo-Velazquez, R. A review of methods for sensing the nitrogen status in plants: Advantages, disadvantages and recent advances. *Sensors* **2013**, *13*, 10823–10843. [[CrossRef](#)]
13. Dordas, C. Nitrogen nutrition index and leaf chlorophyll concentration and its relationship with nitrogen use efficiency in barley (*Hordeum vulgare* L.). *J. Plant Nutr.* **2017**, *40*, 1190–1203. [[CrossRef](#)]

14. Bock, C.H.; Barbedo, J.G.A.; Del Ponte, E.M.; Bohnenkamp, D.; Mahlein, A.-K. From visual estimates to fully automated sensor-based measurements of plant disease severity: Status and challenges for improving accuracy. *Phytopathol. Res.* **2020**, *2*, 9. [[CrossRef](#)]
15. Lowe, A.; Harrison, N.; French, A.P. Hyperspectral image analysis techniques for the detection and classification of the early onset of plant disease and stress. *Plant Methods* **2017**, *13*, 80. [[CrossRef](#)] [[PubMed](#)]
16. Gnyp, M.L.; Miao, Y.; Yuan, F.; Ustin, S.L.; Yu, K.; Yao, Y.; Huang, S.; Bareth, G. Hyperspectral canopy sensing of paddy rice aboveground biomass at different growth stages. *Field Crops Res.* **2014**, *155*, 42–55. [[CrossRef](#)]
17. Stellacci, A.M.; Castrignanò, A.; Troccoli, A.; Basso, B.; Buttafuoco, G. Selecting optimal hyperspectral bands to discriminate nitrogen status in durum wheat: A comparison of statistical approaches. *Environ. Monit. Assess.* **2016**, *188*, 199. [[CrossRef](#)]
18. Zhou, C.; Bucklew, V.G.; Edwards, P.S.; Zhang, C.; Yang, J.; Ryan, P.J.; Hughes, D.P.; Qu, X.; Liu, Z. Portable diffuse reflectance spectroscopy of potato leaves for pre-symptomatic detection of late blight disease. *Appl. Spectrosc.* **2023**, *77*, 491–499. [[CrossRef](#)] [[PubMed](#)]
19. Tian, L.; Wang, Z.; Xue, B.; Li, D.; Zheng, H.; Yao, X.; Zhu, Y.; Cao, W.; Cheng, T. A disease-specific spectral index tracks *Magnaporthe oryzae* infection in paddy rice from ground to space. *Remote Sens. Environ.* **2023**, *285*, 113384. [[CrossRef](#)]
20. West, J.S.; Bravo, C.; Oberti, R.; Moshou, D.; Ramon, H.; McCartney, H.A. Detection of fungal diseases optically and pathogen inoculum by air sampling. In *Precision Crop Protection—The Challenge and Use of Heterogeneity*; Oerke, E.-C., Gerhards, R., Menz, G., Sikora, R.A., Eds.; Springer: Dordrecht, The Netherlands, 2010; pp. 135–149.
21. Oerke, E.-C.; Herzog, K.; Toepfer, R. Hyperspectral phenotyping of the reaction of grapevine genotypes to *Plasmopara viticola*. *J. Exp. Bot.* **2016**, *67*, 5529–5543. [[CrossRef](#)]
22. Berger, K.; Verrelst, J.; Féret, J.-B.; Wang, Z.; Wocher, M.; Strathmann, M.; Danner, M.; Mauser, W.; Hank, T. Crop nitrogen monitoring: Recent progress and principal developments in the context of imaging spectroscopy missions. *Remote Sens. Environ.* **2020**, *242*, 111758. [[CrossRef](#)]
23. Ustin, S.L.; Jacquemoud, S. How the optical properties of leaves modify the absorption and scattering of energy and enhance leaf functionality. In *Remote Sensing of Plant Biodiversity*; Cavender-Bares, J., Gamon, J.A., Townsend, P.A., Eds.; Springer International Publishing: Cham, Switzerland, 2020; pp. 349–384.
24. Mahlein, A.-K. Plant disease detection by imaging sensors—Parallels and specific demands for precision agriculture and plant phenotyping. *Plant Dis.* **2016**, *100*, 241–251. [[CrossRef](#)]
25. Feng, W.; Yao, X.; Zhu, Y.; Tian, Y.C.; Cao, W.X. Monitoring leaf nitrogen status with hyperspectral reflectance in wheat. *Eur. J. Agron.* **2008**, *28*, 394–404. [[CrossRef](#)]
26. Zheng, J.; Song, X.; Yang, G.; Du, X.; Mei, X.; Yang, X. Remote sensing monitoring of rice and wheat canopy nitrogen: A review. *Remote Sens.* **2022**, *14*, 5712. [[CrossRef](#)]
27. Bauriegel, E.; Giebel, A.; Geyer, M.; Schmidt, U.; Herppich, W.B. Early detection of *Fusarium* infection in wheat using hyperspectral imaging. *Comput. Electron. Agric.* **2011**, *75*, 304–312. [[CrossRef](#)]
28. Mahlein, A.-K.; Steiner, U.; Hillnhütter, C.; Dehne, H.-W.; Oerke, E.-C. Hyperspectral imaging for small-scale analysis of symptoms caused by different sugar beet diseases. *Plant Methods* **2012**, *8*, 3. [[CrossRef](#)] [[PubMed](#)]
29. Kobayashi, T.; Sasahara, M.; Kanda, E.; Ishiguro, K.; Hase, S.; Torigoe, Y. Assessment of rice panicle blast disease using airborne hyperspectral imagery. *Open Agric. J.* **2016**, *10*, 28–34. [[CrossRef](#)]
30. Zhang, G.; Xu, T.; Tian, Y.; Feng, S.; Zhao, D.; Guo, Z. Classification of rice leaf blast severity using hyperspectral imaging. *Sci. Rep.* **2022**, *12*, 19757. [[CrossRef](#)] [[PubMed](#)]
31. Maina, A.W.; Oerke, E.-C. Characterization of rice–*Magnaporthe oryzae* interactions by hyperspectral imaging. *Plant Dis.* **2023**, *107*, 3139–3147. [[CrossRef](#)] [[PubMed](#)]
32. Devadas, R.; Lamb, D.W.; Simpfendorfer, S.; Backhouse, D. Evaluating ten spectral vegetation indices for identifying rust infection in individual wheat leaves. *Precis. Agric.* **2009**, *10*, 459–470. [[CrossRef](#)]
33. Zhao, Y.-R.; Li, X.; Yu, K.-Q.; Cheng, F.; He, Y. Hyperspectral imaging for determining pigment contents in cucumber leaves in response to angular leaf spot disease. *Sci. Rep.* **2016**, *6*, 27790. [[CrossRef](#)] [[PubMed](#)]
34. Liu, W.; Sun, C.; Zhao, Y.; Xu, F.; Song, Y.; Fan, J.; Zhou, Y.; Xu, X. Monitoring of wheat powdery mildew under different nitrogen input levels using hyperspectral remote sensing. *Remote Sens.* **2021**, *13*, 3753. [[CrossRef](#)]
35. Tartachnyk, I.I.; Rademacher, I.; Kühbauch, W. Distinguishing nitrogen deficiency and fungal infection of winter wheat by laser-induced fluorescence. *Precis. Agric.* **2006**, *7*, 281–293. [[CrossRef](#)]
36. Markwell, J.; Osterman, J.C.; Mitchell, J.L. Calibration of the Minolta SPAD-502 leaf chlorophyll meter. *Photosynth. Res.* **1995**, *46*, 467–472. [[CrossRef](#)]
37. Savitzky, A.; Golay, M.J.E. Smoothing and differentiation of data by simplified least squares procedures. *Anal. Chem.* **1964**, *36*, 1627–1639. [[CrossRef](#)]
38. Kruse, F.A.; Heidebrecht, K.B.; Shapiro, A.T.; Barloon, P.J.; Goetz, A.F.H. The spectral image processing system (SIPS) interactive visualization and analysis of imaging spectrometer data. *Remote Sens. Environ.* **1993**, *44*, 145–163. [[CrossRef](#)]
39. Guyot, G.; Baret, F.; Major, D.J. High spectral resolution: Determination of spectral shifts between the red and the near infrared. *Int. Arch. Photogram. Remote Sens.* **1988**, *11*, 750–760.
40. Gelfond, J.; Goros, M.; Hernandez, B.; Bokov, A. A System for an accountable data analysis process in R. *R J.* **2018**, *10*, 6. [[CrossRef](#)]

41. Fageria, N.K.; De Morais, O.P.; Dos Santos, A.B. Nitrogen use efficiency in upland rice genotypes. *J. Plant Nutr.* **2010**, *33*, 1696–1711. [[CrossRef](#)]
42. Gholizadeh, A.; Saberioon, M.; Borůvka, L.; Wayayok, A.; Mohd Soom, M.A. Leaf chlorophyll and nitrogen dynamics and their relationship to lowland rice yield for site-specific paddy management. *Inf. Process. Agric.* **2017**, *4*, 259–268. [[CrossRef](#)]
43. Huang, J.; He, F.; Cui, K.; Buresh, R.J.; Xu, B.; Gong, W.; Peng, S. Determination of optimal nitrogen rate for rice varieties using a chlorophyll meter. *Field Crops Res.* **2008**, *105*, 70–80. [[CrossRef](#)]
44. Ata-Ul-Karim, S.T.; Cao, Q.; Zhu, Y.; Tang, L.; Rehmani, M.I.A.; Cao, W. Non-destructive assessment of plant nitrogen parameters using leaf chlorophyll measurements in rice. *Front. Plant Sci.* **2016**, *7*, 1829. [[CrossRef](#)]
45. Schlemmer, M.; Gitelson, A.; Schepers, J.; Ferguson, R.; Peng, Y.; Shanahan, J.; Rundquist, D. Remote estimation of nitrogen and chlorophyll contents in maize at leaf and canopy levels. *Int. J. Appl. Earth Obs. Geoinf.* **2013**, *25*, 47–54. [[CrossRef](#)]
46. Peng, S.; Garcia, F.V.; Laza, R.C.; Sanico, A.L.; Visperas, R.M.; Cassman, K.G. Increased N-use efficiency using a chlorophyll meter on high-yielding irrigated rice. *Field Crops Res.* **1996**, *47*, 243–252. [[CrossRef](#)]
47. Friedel, M.; Hendgen, M.; Stoll, M.; Löhnertz, O. Performance of reflectance indices and of a handheld device for estimating in-field the nitrogen status of grapevine leaves. *Aust. J. Grape Wine Res.* **2020**, *26*, 110–120. [[CrossRef](#)]
48. Rubo, S.; Zinkernagel, J. Exploring hyperspectral reflectance indices for the estimation of water and nitrogen status of spinach. *Biosyst. Eng.* **2022**, *214*, 58–71. [[CrossRef](#)]
49. Ballini, E.; Nguyen, T.T.; Morel, J.-B. Diversity and genetics of nitrogen-induced susceptibility to the blast fungus in rice and wheat. *Rice* **2013**, *6*, 32. [[CrossRef](#)] [[PubMed](#)]
50. Talukder, Z.I.; McDonald, A.J.S.; Price, A.H. Loci controlling partial resistance to rice blast do not show marked QTL × environment interaction when plant nitrogen status alters disease severity. *New Phytol.* **2005**, *168*, 455–464. [[CrossRef](#)]
51. Frontini, M.; Boissard, A.; Frouin, J.; Ouikene, M.; Morel, J.B.; Ballini, E. Genome-wide association of rice response to blast fungus identifies loci for robust resistance under high nitrogen. *BMC Plant Biol.* **2021**, *21*, 99. [[CrossRef](#)]
52. Osuna-Canizalez, F.J.; De Datta, S.K.; Bonman, J.M. Nitrogen form and silicon nutrition effects on resistance to blast disease of rice. *Plant Soil* **1991**, *135*, 223–231. [[CrossRef](#)]
53. Snoeijers, S.S.; Perez-Garcia, A. The effect of nitrogen on disease development and gene expression in bacterial and fungal plant pathogens. *Eur. J. Plant Pathol.* **2000**, *106*, 493–506. [[CrossRef](#)]
54. Leucker, M.; Mahlein, A.-K.; Steiner, U.; Oerke, E.-C. Improvement of lesion phenotyping in *Cercospora beticola*–sugar beet interaction by hyperspectral imaging. *Phytopathology* **2016**, *106*, 177–184. [[CrossRef](#)] [[PubMed](#)]
55. Sanaeifar, A.; Yang, C.; De La Guardia, M.; Zhang, W.; Li, X.; He, Y. Proximal hyperspectral sensing of abiotic stresses in plants. *Sci. Total Environ.* **2023**, *861*, 160652. [[CrossRef](#)] [[PubMed](#)]
56. Laroche-Pinel, E.; Albughdadi, M.; Duthoit, S.; Chéret, V.; Rousseau, J.; Clenet, H. Understanding vine hyperspectral signature through different irrigation plans: A first step to monitor vineyard water status. *Remote Sens.* **2021**, *13*, 536. [[CrossRef](#)]

Disclaimer/Publisher’s Note: The statements, opinions and data contained in all publications are solely those of the individual author(s) and contributor(s) and not of MDPI and/or the editor(s). MDPI and/or the editor(s) disclaim responsibility for any injury to people or property resulting from any ideas, methods, instructions or products referred to in the content.